Journal of Materials Chemistry A

Accepted Manuscript

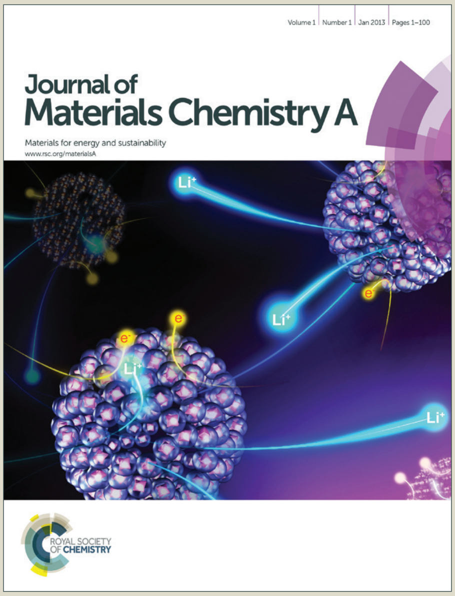

ROYAL SOCIETY OF CHEMISTRY

www.rsc.org/materialsA

TOC figure and text

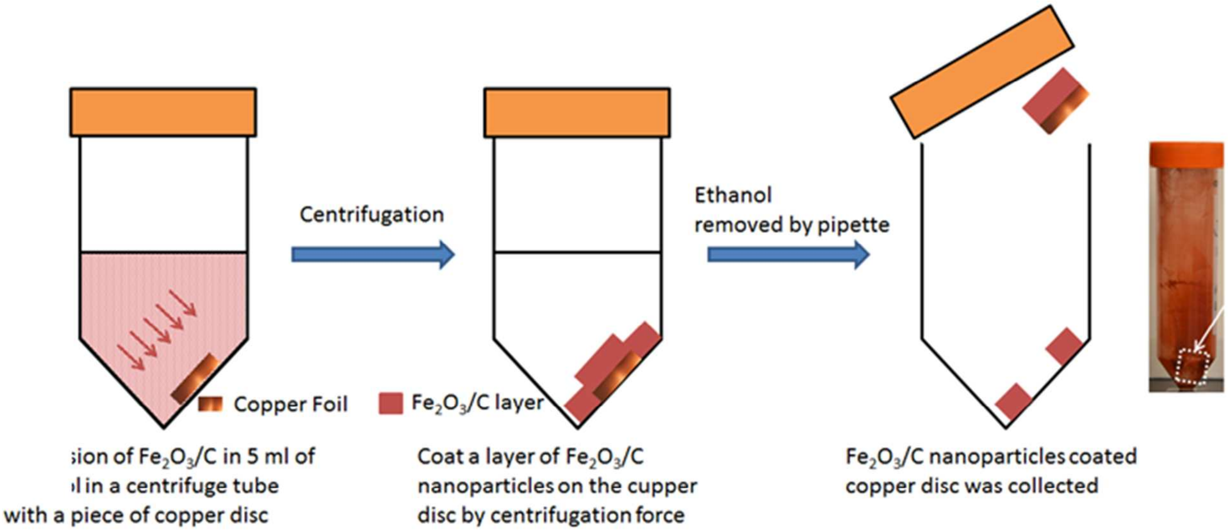

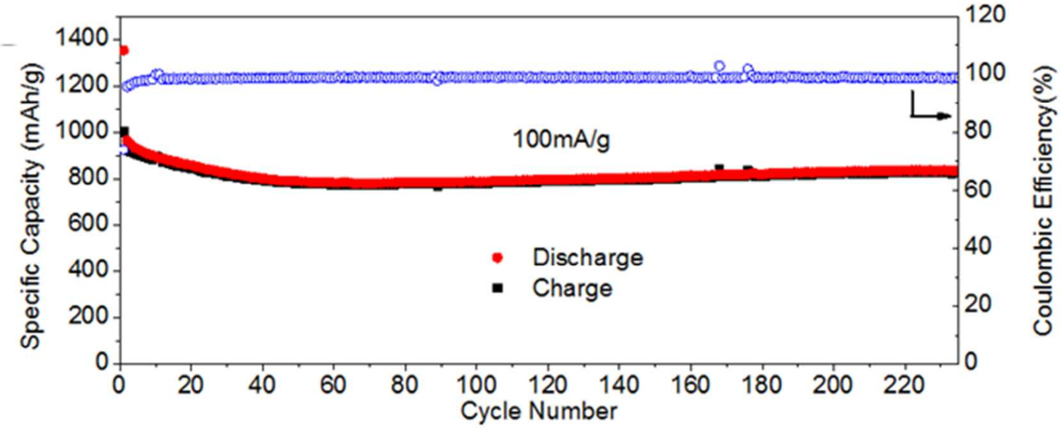

Additive-free porous olive-like carbon decorated Fe_3O_4 based electrodes with active materials directly synthesized on the current collectors by centrifugation assisted deposition (CAD) was developed. Excellent cycling performance was achieved with a specific capacity at ~ 800 mA h g^{-1} for at least 235 cycles and impressive rate performance was accomplished.

Porous Olive-Like Carbon Decorated Fe_3O_4 Based Additive-Free Electrode for Highly Reversible Lithium Storage

*Jian Zhu, K.Y. Simon Ng, Da Deng**

Department of Chemical Engineering and Materials Science, Wayne State University,

5050 Anthony Wayne Dr, Detroit, Michigan, United States, 48202

*E-mail:da.deng@wayne.edu

Abstract

Porous nanostructured olive-like carbon decorated Fe_3O_4 (Fe_3O_4/C) were prepared via *in-situ* carbothermal treatment of porous olive-like composite of Fe_2O_3/C. The precursor of porous olive-like Fe_2O_3/C nanoparticles was prepared through an ultrafast (75 min) one-pot solvothermal method. The porous olive-like Fe_3O_4/C and its precursor of Fe_2O_3/C nanostructures were formed by aggregation of orderly aligned nanorods as building subunits. The successful conversion from Fe_2O_3/C to Fe_3O_4/C by *in situ* carbothermic partial reduction was evidenced by extensive characterization. Additionally, a novel centrifugation-assisted procedure (CAP) to prepare additive-free Fe_3O_4 based electrodes with active materials directly synthesized on the current collector was developed for the first time. The porous olive-like Fe_2O_3/C nanoparticles dispersed in ethanol was coated on Cu current collectors by centrifugation-assisted deposition (CAD) directly without any additives employed and subsequently heated to convert to Fe_3O_4/C coated Cu disc which can be used as an electrode without any further process. In contrast, traditional electrode preparation involves multiple steps of slurry preparation, coating, drying in vacuum oven and additives (e.g., PVDF binder, carbon black conductivity enhancer and NMP solvent) are employed in the process. The as-prepared additive-free porous Fe_3O_4/C based electrode exhibited superior electrochemical performances in lithium storage. Excellent cycling performance was achieved with a specific capacity at ~ 800 mA h g^{-1} for at least 235 cycles. Impressive rate performance was accomplished when tested under different currents: no significant capacity drop observed when current was doubled and a specific capacity of 730 mA h g^{-1} could be maintained at current of 1500 mA g^{-1}.

Keywords: Carbon decorated Fe3O4; additive-free; anode; carbothermic reduction; lithium ion batteries.

1. Introduction

Rechargeable lithium-ion batteries (LIBs) have been attracting much attention in the past few decades. LIBs with high power and energy density are highly desirable in order to meet the increasing demand for energy storage, in particular, electric vehicles.[1-4] Currently, LIBs still exclusively use carbon as negative-electrode materials for its good cycling performance based on intercalation/deintercalation mechanism of Li storage. However, the theoretical capacity of graphite at 372 mA h g^{-1} (based on LiC_6) has almost been achieved. On the other hand, the intercalation of lithium into graphite mainly occurs at low potential close to zero V (vs. Li/Li^+). Accidental overcharge at high currents may lead to possible formation of lithium dendrites that short circuit anode and cathode and cause thermal runaway or even a fire. Recently, much attention has been devoted to develop carbon-alternative negative-electrode materials, which must have higher specific capacity and better safety performance than widely adopted carbon anode.[1, 3-6]

Various metal oxides have been extensively explored as carbon-alternatives, in particular, magnetite Fe_3O_4.[3, 5, 7-9] Fe_3O_4 has a theoretical capacity of 927 mA h g^{-1} and its potential of lithium insertion based on conversion-type mechanism is significantly higher compared to that of carbon. Other advantages are low cost, abundance, environmental friendliness, and especially the high electrical conductivity at room temperature of about 2.5×10^2 S/cm.[10] High electrical conductivity is rarely observed in other metal oxides investigated for application in LIBs (e.g. α-Fe_2O_3 has an electrical conductivity of ~10^{-4} S/cm，which is six order of magnitude or x10^{-6} lower than magnetite). High conductivity is highly desirable for electrodes in LIBs to facilitate charge transfer.[11, 12] However, as one of the conversion-type negative-electrode materials, the volume expansion (~200%) of magnetite[13] is much larger than that of insertion-type negative-electrode materials (e.g., graphite) upon lithium insertion. This huge volume variation or pulverization could cause disintegration of the electrode and lead to poor cycling performance. This poor cyclability becomes one of the obstacles to commercialize Fe_3O_4 as negative-electrode materials in LIBs. On the other hand, based on the conversion-type lithium storage mechanism, Fe^0 nanograins will be generated through electrochemical reduction.[12] Fe^0 nanograins are highly reactive toward the organic electrolyte. The irreversible reactions on the surface of Fe^0 nanograins with the electrolyte could also cause poor cycling performance.[11] To address the poor cycling performance of Fe_3O_4, one strategy is to adopt nanoscale materials to buffer the volume variation during charge/discharge process.[11-17] The other strategy is to add or coat with carbon to minimize the exposure between Fe^0 nanograins and organic electrolyte as well as to increase the electrical conductivity. For example, Fe_3O_4@C composites have been demonstrated to achieve certain level of success in terms of electrochemical performances.[18-23] The composites includes Fe_3O_4@C nanospindles,[15] Fe_3O_4@C nanorings,[23] C-encapsulated Fe_3O_4 nanoparticles homogeneously embedded in porous graphitic carbon nanosheets.[24] Lou et al. reported a series of nanostructured iron oxide based anode materials for LIBs,[25] such as carbon coated Fe_2O_3 nanorods,[26] nanocubes,[27] microboxes,[28, 29] nanotubes,[30] nanodiscs,[31] nanospheres,[32] hollow microspheres of Fe_3O_4,[33] nanohorns on CNTs,[34] and Fe_3O_4 nanospheres with carbon matrix.[35] Therefore, Fe_3O_4 could find promising application as negative electrodes in LIBs.

Herein, we reported a procedure to prepare porous olive-like carbon decorated Fe_3O_4 based additive-free electrodes with improved electrochemical performances. The precursor of porous Fe_2O_3/C with olive-like particles obtained via ultrafast (75 min) one-pot synthesis were constructed by aggregation of short nanorods with length of ~18 nm and width of ~8 nm. It is particularly interesting to highlight that a novel centrifugation-assisted deposition (CAD) method was developed to prepare additive-free carbon decorated Fe_3O_4 where active materials were directly prepared on the current collector. In another word, once the synthesis of active materials finished, the electrodes are ready. No binder, conductivity enhancer or solvent were employed. The electrodes could be direct assembled into cells without any post-synthesis processing. In contrast, traditional electrode preparation involves multiple steps of slurry preparation, coating, drying in vacuum oven and additives (e.g., PVDF binder, carbon black conductivity enhancer and NMP solvent) are employed in the process, in addition to the conventional procedures to prepare the active electrode materials. The as-prepared additive-free porous carbon decorated Fe_3O_4 based electrodes exhibited superior electrochemical performances in LIBs. A specific capacity of 800 mA h g^{-1} could be maintained for at least 235 cycles with minimum capacity fading. Moreover, it exhibited excellent rate performance: specific capacities of 761, 752, and 727 mA h g^{-1} were achieved at high currents of 500, 1000 and 1500 mA g^{-1}, respectively. The results suggest that the binder-free carbon decorated Fe_3O_4 based electrode obtained by CAP could be potentially used in high-rate LIBs.

2. Experimental Section

Preparation olive-like Fe_2O_3/C composite as precursor: In a typical synthesis, 0.4 mmol of $FeCl_3\cdot 6H_2O$ and 0.4 mmol of D-glucose were fully dissolved in 16 ml of deionized water, and 0.4 mmol of dimethyl oxalate was fully dissolved in 16 ml of 1-propanol. The former solution was added drop by drop into the later solution. The mixture was stirred for 15 min, and then transferred into a 45 ml Teflon-lined autoclave and heated at 200 °C for 75 min. The solid products were collected and washed repeatedly with water and ethanol, and dried at 80°C in a vacuum oven overnight.

Preparation of additive-free ready electrode of olive-like carbon decorated Fe_3O_4: Typically, calculated amount of olive-like Fe_2O_3/C powders were dispersed into 5 ml of ethanol in a 50 ml centrifuge tube under ultrasonic to achieve a highly homogeneous suspension. A piece of clean copper disc typically used as a current collector was placed into the centrifuge tube and was centrifuged together with the mixture solution at 6000 rpm for 5 min. The olive-like Fe_2O_3/C nanoparticles were deposited by centrifugal force and coated firmly on only one side of the copper disc (Figure S1 in supporting information (SI)). The olive-like Fe_2O_3/C coated copper disc was dried in a vacuum oven at 80 ^{o}C overnight. To prepare olive-like carbon decorated Fe_3O_4 based electrode, the coated copper disc was sintered in a tube furnace at a heating rate of 6 ^{o}C /min to 600 ^{o}C and maintained at the set temperature for 2 h under argon. The overall process and changes in compositions are illustrated in Scheme 1.

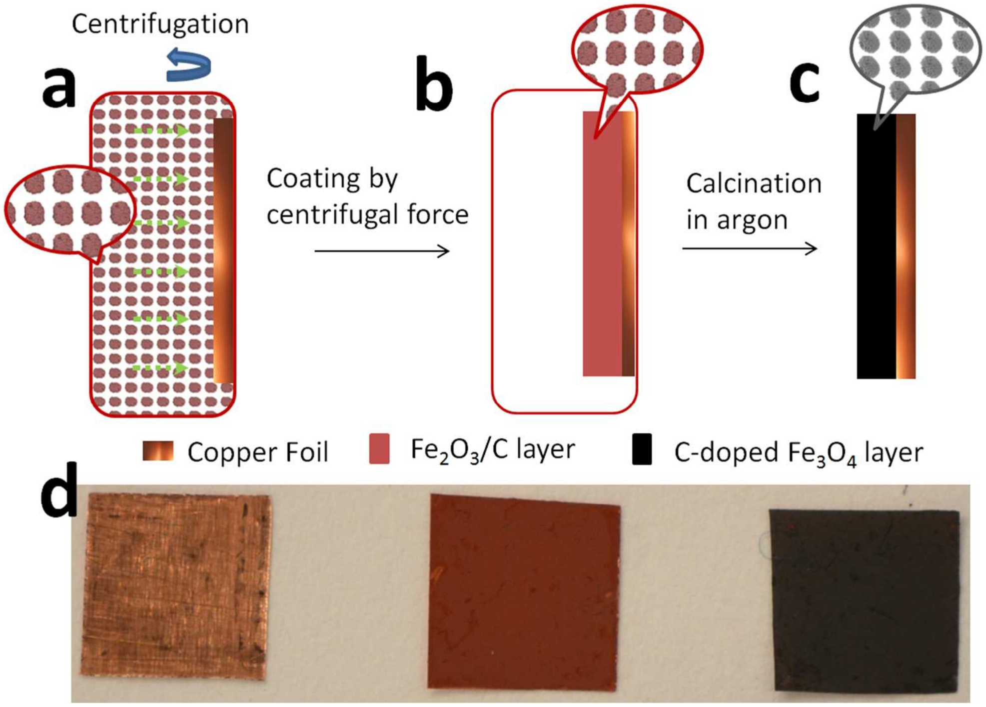

Scheme 1. Schematic of the CAP we developed to make additive-free electrode of olive-like carbon decorated Fe_3O_4: (a) precursor of Fe_2O_3/C nanoparticles dispersed in ethanol is coated on

a Cu disc under centrifugation; (b) A layer of Fe_2O_3/C nanoparticles coated on only one side of the Cu disc; (c) A layer of carbon decorated Fe_3O_4 nanoparticles coated the Cu disc obtained by heating (b) in argon; (d) the corresponding optical image of the Cu discs at each step of treatment: from the left to the right, bare → Fe_2O_3/C layer coated → carbon decorated Fe_3O_4 layer coated Cu discs. Note: the other sides of those coated Cu discs were not coated by our method due to one-side deposition by centrifugation, Figure S2 in SI.

Characterization: Powder X-ray diffraction (XRD) was carried out with a Rigaku Smartlab X-ray diffractometer using Cu K_α radiation (λ=0.15418 nm). The morphology of the materials was characterized by field emission scanning electron microscopy (JSM-7600 FE SEM, with accelerating voltage of 15 kV) and by transmission electron microscopy (JEOL 2010 TEM instrument, with accelerating voltage of 200 kV). The energy-dispersive X-ray spectroscopy (EDS) was measured using Pegasus Apex 2 integrated EDS. Thermal gravimetric analysis (TGA) was carried out with SDT Q600 (TA Instruments) under dynamic air atmosphere with a ramping rate of 10^{o}C/min to 900^{o}C.

Electrochemical Measurements: The additive-free electrodes of olive-like carbon decorated Fe_3O_4 coated on copper disc as obtained by CAP were assembled into testing cells directly. Electrochemical test cells were assembled in an argon-filled glove box using the additive-free electrode as the working electrode, metallic lithium foil as the counter and reference electrode, 1 M solution of $LiPF_6$ in a 50:50 v/v mixture of ethylene carbonate (EC) and diethyl carbonate (DEC) as the electrolyte, and PP/PE/PP trilayer membranes (Celgard 2320) as the separator. The cells were charged and discharged galvanostatically at room temperature in the voltage window of 0.01V-3V at different currents on a MTI BST8-WA battery tester.

3. Results and Discussions

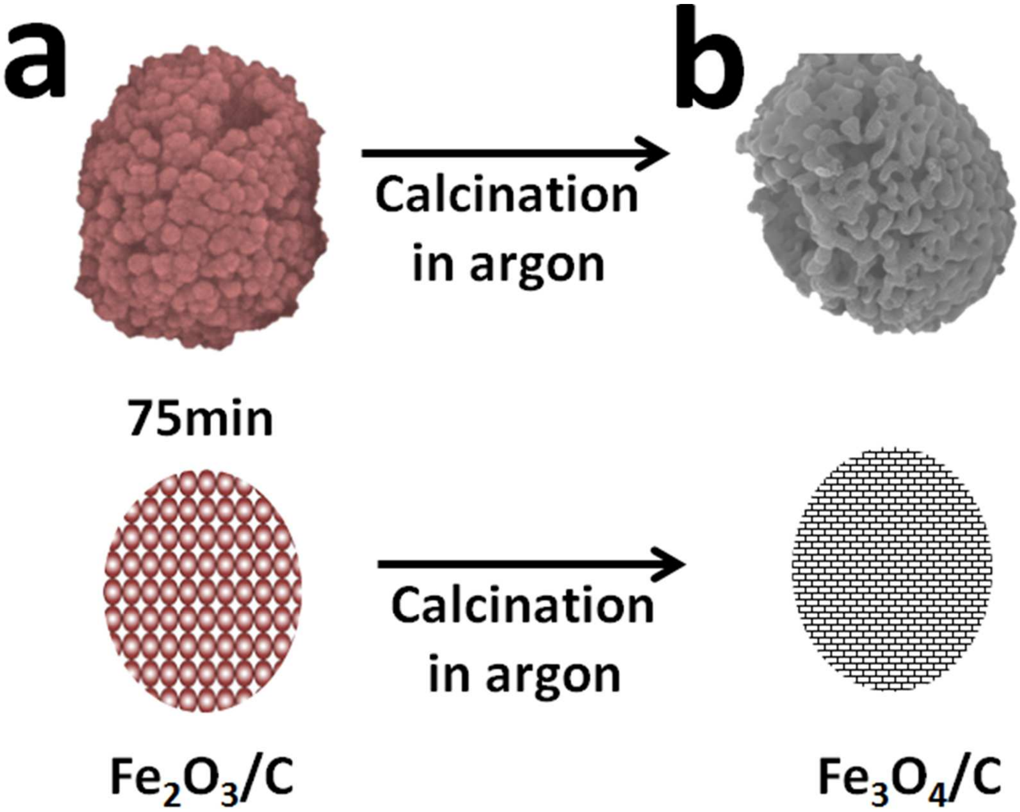

Figure 1. Schematic illustration of the change in composition from Fe_2O_3/C to carbon decorated Fe_3O_4: (a) porous olive-like Fe_2O_3/C obtained through solvothermal process after reaction time of 75 min. (b) porous olive-like carbon decorated Fe_3O_4 from partial carbonthermic reduction of Fe_2O_3 by carbon under calcination in argon.

The overall preparation process and change in compostion of materials are shown in Scheme 1 and Figure 1. Porous olive-like Fe_2O_3/C nanoparticles as precursors were prepared after 75 min of solvothermal reaction, as shown in Figure 1a. The porous olive-like carbon decorated Fe_3O_4 nanoparticles with rough surfaces were obtained by calcinating porous olive-like Fe_2O_3/C precursor undere the protection of argon, as shown in Figure 1b. Here the carbon inside the precursor of olive-like Fe_2O_3/C played an important role to partially reduce Fe_2O_3 to Fe_3O_4 under calcinating porous olive-like Fe_2O_3/C due to carbothermic reactions.

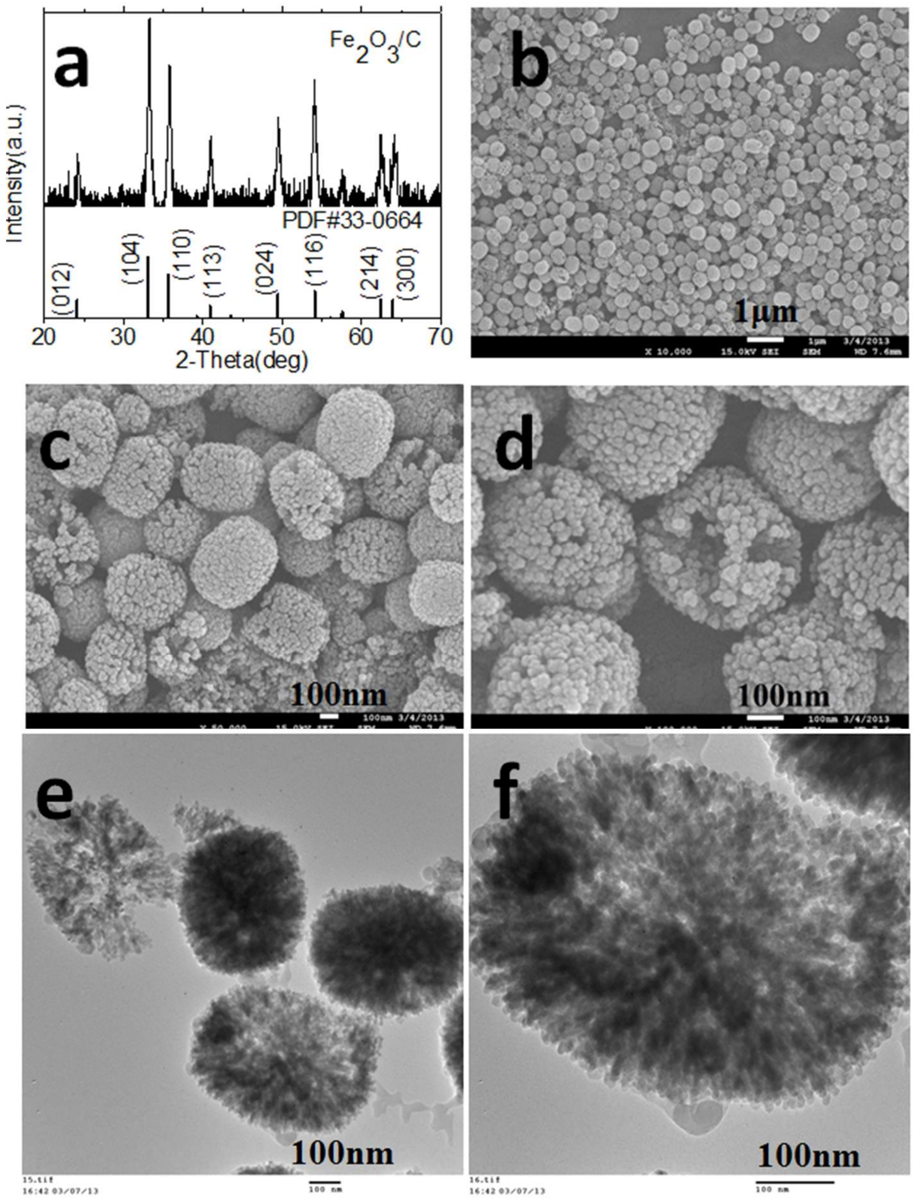

Figure 2. Characterization of the precursor of olive-like porous Fe_2O_3/C: (a) XRD pattern; (b) low-magnification FESEM image overall view; (c) high-magnification view of few typical olive-like porous Fe_2O_3/C nanoparticles; (d) zoom-in view showing a broken particle with the internal structure of nanorod aggregates revealed; (e) TEM images of few typical olive-like Fe_2O_3/C nanoparticles; (f) zoom-in view showing the building units of nanorods.

Structure of porous olive-like Fe_2O_3/C

Porous olive-like Fe_2O_3/C nanoparticles, the precursor for making carbon decorated Fe_3O_4, were prepared through a fast solvothermal reaction with reaction time of only 75 min and characterized by XRD, FESEM and TEM (Figure 2). The XRD pattern of as-prepared precursor can be indexed to α-Fe_2O_3 with rhombohedral structure (JCPDS Card No. 33-0664) and no impurities are detected in the pattern (Figure 2a). The crystalline size calculated from Scherrer equation based on (110) peaks is 18 nm, which is in accordance with the size of building subunits observed under FESEM and TEM (Figure 2d&f). The absence of carbon peaks suggests that the carbon from hydrothermally carbonized glucose is mainly amorphous.[36] The EDS (Figure S3a in SI) exhibits that the as-prepared particles contain the elements of carbon, iron and oxygen as expected. Carbon was produced through the carbonization of glucose during the solvothermal process above 160°C, which is well documented.[15, 23, 36-38] Typical morphology and structure of the olive-like Fe_2O_3/C nanoparticles are clearly revealed by the FESEM images (Figure 2b-d). The overall morphology and size distribution of the olive-like Fe_2O_3/C nanoparticles are revealed by low-magnification FESEM image (Figure 2b). The aspect ratio of the olive-like structure is around 3:2, as shown in high-magnification image (Figure 2c). The olive-like α-Fe_2O_3/C nanoparticles are about 300-600 nm in length and 200-400 nm in diameter. More details of the internal structure of the nanoparticle are shown in the zoom-in view FESEM image (Figure 2d): the olive-like nanoparticle is formed by aggregation of ordered small nanorods with length of ~18 nm and width of ~8 nm (which was further confirmed by TEM). A broken olive-like structure at the center of the high-magnification FESEM image shows that the whole structure is highly porous, from the core to the surface. The structure of the α-Fe_2O_3/C composite is further revealed by the TEM characterization (Figure 2e-f).

Effect of experimental parameters on olive-like Fe_2O_3/C nanoparticles

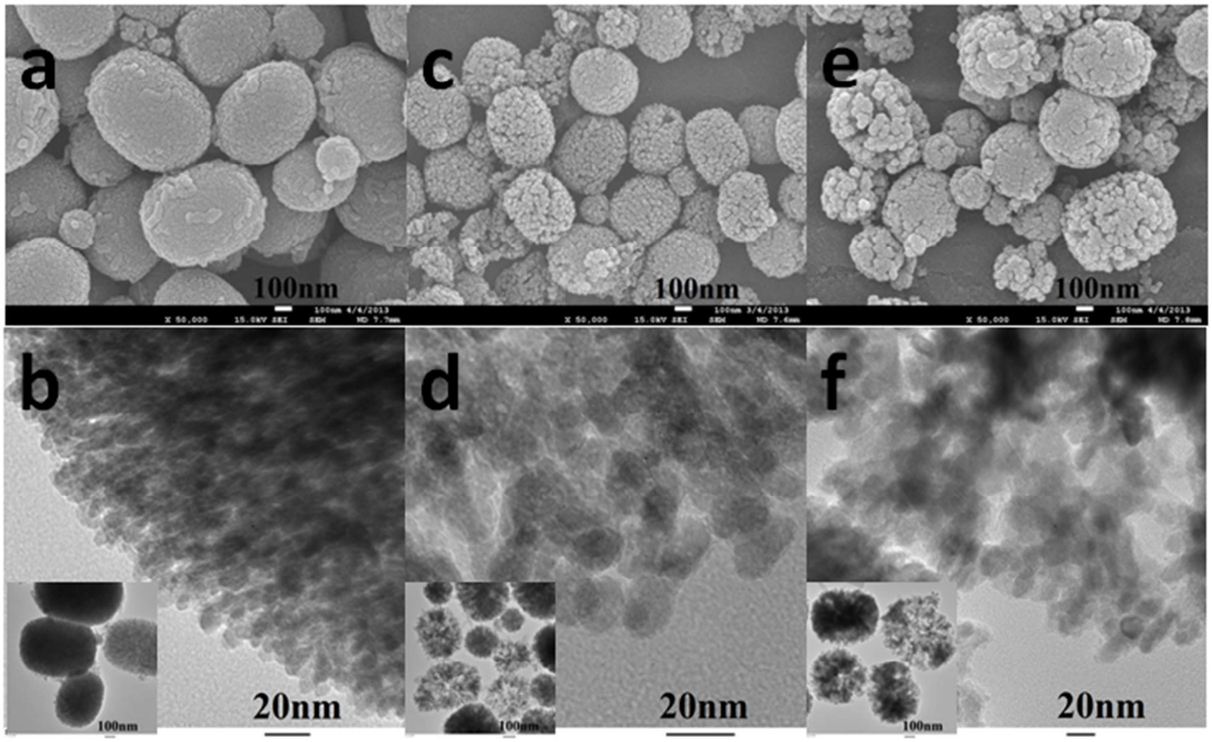

Figure 3. Effect of reaction time: FESEM images (top row) and TEM images (bottom row) of olive-like Fe_2O_3/C nanoparticles prepared with different reaction times of (a, b) 45 min, (c, d) 75 min and (e, f) 3 h. Insets of (b,d,f) are corresponding low-magnification TEM images.

A set of experiments were carried out to study the effect of reaction times on the structure of the olive-like Fe_2O_3/C precursors. Those nanoparticles obtained at different reaction times were characterized by FESEM and TEM (Figure 3). When the reaction time was 45 min, less porous olive-like nanoparticles were formed (Figure 3a&b and the inset of 3b). The nanorod subunits, with length and width of around 18 and 8 nm, respectively, were aggregated to form the olive-like structure and closely packed (Figure 3b). All the subunits of nanorods are well aligned in the same way, radiating from the core to the outside, as shown in Figure 3b. As reaction time increased from 45 min to 75 min, the olive-like structure became more porous, as evidenced by the more distinguishable gaps between fat nanorod subunits in Figure 3c and 3d. The inset of

Figure 3d reveals that the whole olive-like structure is porous, which is consistent with the broken olive-like structure observed in high magnification FESEM image (Figure 2d). As reaction time further increased to 3 h, the porous nature was preserved, as shown in Figure 3e and inset of Figure 3f. However, with longer reaction time, the length and diameter of the nanorod subunits increase to ~23 and 10 nm, respectively. Also, the orientations of the subunits are more random, as compared to the samples prepared with shorter reaction times of 45 and 75 min.

Besides the reaction time, the porosity and the shape of the as-prepared olive-like structure can be affected by the amount of glucose (Figure S4 in SI). With 0.4 mmol (Figure S4 a-b in SI) or 0.2 mmol (Figure S4 c-d in SI), the olive-like structures are highly porous with the nanorods as the basic building units. Occasionally, by-products of hollow nanoparticles were also observed (Figure S4c in SI). For comparison, with only 0.1 mmol glucose (Figure S4 e-f in SI), the porosity of the olive-like structure is less than those obtained with 0.4 mmol or 0.2 mmol of glucose. A tunnel which connects the two ends of olive-like structure and two open ends, instead of highly porous structure was observed. We observed that the aspect ratio of as the prepared olive-like nanoparticles could be tuned through the control of amount of glucose. The aspect ratio increases from ~3:2 to 2:1 when the amount of glucose added in decreased from 0.4 mmol to 0.1 mmol. Without any glucose, cocoon-like hollow structure with aspect ratio of ~2.5:1 could be achieved. [9] We proposed that the amount of glucose could affect the aggregation of subunits leading to different structure of the aggregates. However, the fundamental explanation is still not clear at this time.

Based on the experimental observation, a plausible formation mechanism is proposed. The formation of porous olive-like nanoparticles starts from hydrolysis of Fe^{3+} ions and nucleation in solution and subsequently forms nanorods.[9] The nanorods as building units aggregate to form olive-like structure and the nanorods are densely packed initially (Figure 3a). The highly porous olive-like aggregates form with longer reaction time (Figure 3b). The small nanorod subunits, which possess higher surface energy in solution, tend to be dissolved more easily to minimize total surface energy. Thus, the big nanorods grow with the continuing dissolving of small subunits and re-deposition on large subunits. With the decrease of number of small nanorods and the increase of size of the large nanorods, void spaces are generated and the particles become porous. Meanwhile, the aspect ratio and the porosity can be tuned through the control of glucose. It might due to that the glucose or the deposited carbon may influence the surface property of the nanorod subunits and their aggregation. Thus, the orientated alignment of subunits could be different from those in the system without glucose.[9] Our current ongoing effort is to systematically study the effects of experimental parameters and further understand the formation mechanism.

Structure of the olive-like carbon decorated Fe_3O_4

The as-prepared olive-like Fe_2O_3/C could be converted to carbon decorated Fe_3O_4 preserving the overall morphology well. The successful partial reduction of Fe_2O_3 was proved by the evidence that Fe_3O_4 was produced as revealed by XRD (Figure 4a). All the peaks of the XRD pattern can be assigned to Fe_3O_4 (JCPDS Card No.75-0449), and no peak of α-Fe_2O_3 is observed, suggesting that carbothermic conversion of Fe_2O_3 into Fe_3O_4 was successful and complete. The crystalline sizes of as prepared Fe_3O_4 are 45 nm, calculated based on (220) peak, which is significantly larger than the crystallite size of the Fe_2O_3 precursor at around ~ 20 nm. The typical black color of Fe_3O_4,[15, 39] rather than the typical red color of Fe_2O_3, was obtained and all the black power of olive-like carbon decorated Fe_3O_4 attracted by a magnetic bar (Figure 4b), demonstrate that Fe_2O_3 was successfully converted to Fe_3O_4. Note that the powder of carbon decorated Fe_3O_4 was obtained without being coated on copper disc by CAP in this case and the precursor powder was heat treated similarly under agron in a crucible. The conversion from Fe_2O_3 to Fe_3O_4 under inert gas also proves the existence of carbon produced by the solvothermal carbonization of glucose, which acts as the only reducing agent to convert Fe_2O_3 to Fe_3O_4.

The morphology of as-synthesized olive-like carbon decorated Fe_3O_4 was revealed by FESEM and TEM images in Figure 4 c-f. After the calcination at 600 ^oC under Ar, the olive-like structure was maintained (Figure 4c and 4d). The porosity of the olive-like carbon decorated Fe_3O_4 is also preserved, revealed by the broken olive-like structure in Figure 4d. The size of subunits of carbon decorated Fe_3O_4 increased to around 50 nm from 18 nm of those in size of subunits in precursor of Fe_2O_3/C (Figure 4e and 4f), which is in consistent with the sizes estimated from the XRD. The increase in size of subunits can be attributed to the high temperature annealing induced crystalline growth. As compared to the precursor of Fe_2O_3/C aggregates assembled by aligned nanorods, carbon decorated Fe_3O_4 was constructed by joined subunits. The connection of building subunits may be attributed to the annealing process where subunits are joined by grain boundary diffusions which was also observed in the study of other metal oxide nanomaterials.[40] It may also be attributed to the consumption of carbon in Fe_2O_3 through the carbothermic reduction process which eliminates the impurities between grain boundaries. The SAED pattern (the inset of Figure 4e) demonstrates that the olive-like carbon decorated Fe_3O_4 is crystalline with all the diffraction spots can be assigned to Fe_3O_4.

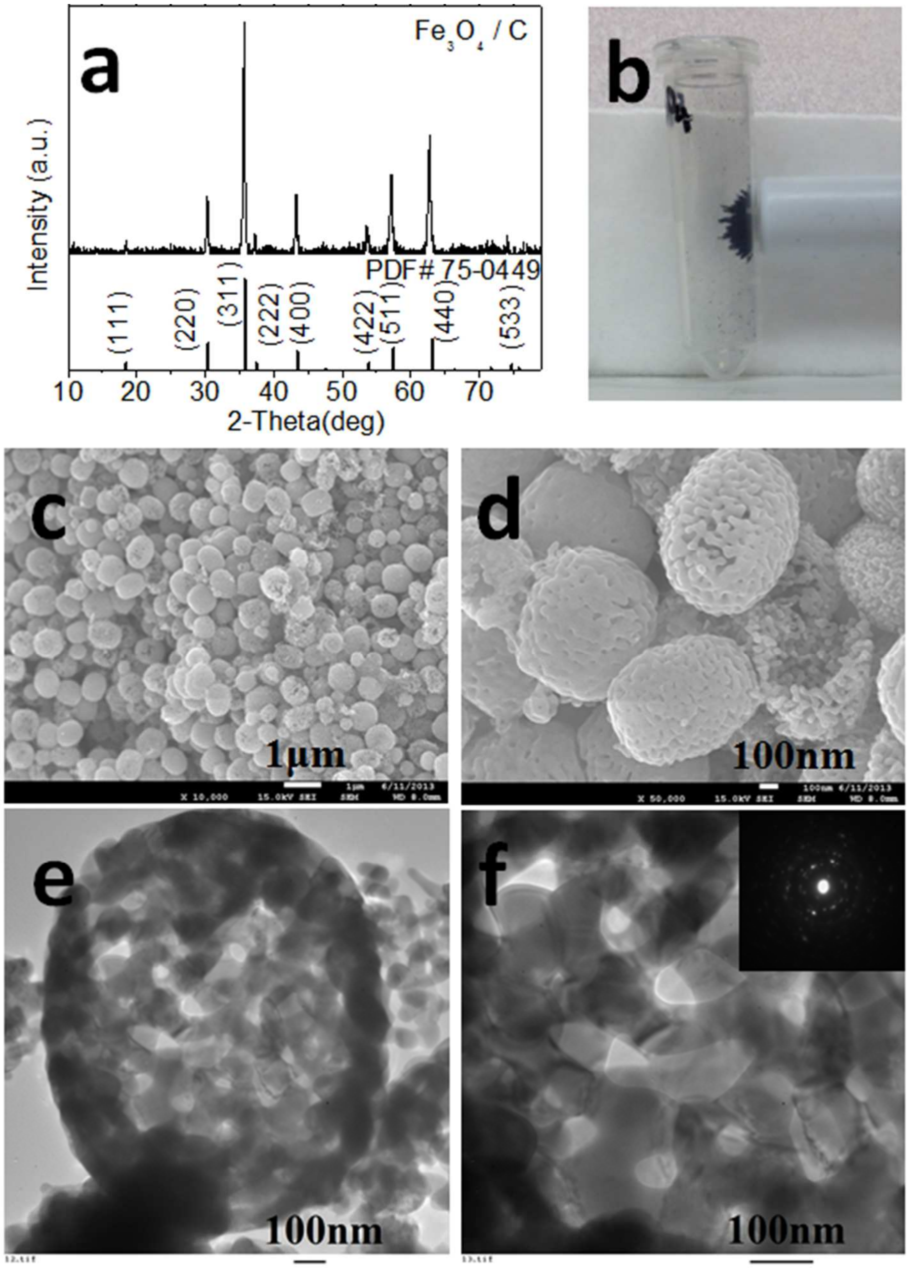

Figure 4. Characterization of the olive-like carbon decorated Fe_3O_4 obtained by *in situ* carbothermic conversion from Fe_2O_3/C: (a) XRD pattern; (b) optical image shows the black colored carbon decorated Fe_3O_4 and its magnetic property; FESEM images at (c) low-magnification overall view, and (d) high-magnification view of few typical particles; TEM images of (e) a typical carbon decorated Fe_3O_4 olive-like nanoparticle, and (f) zoom-in view of a

section of (e) showing the building subunits. Inset of (f) is the typical SAED pattern of crystalline Fe_3O_4.

The carbon content in the as-prepared Fe_3O_4/C materials is quantitatively determined by the TGA analysis (Figure S5 in SI). The small weight loss below 150 ^oC was due to the evaporation of the adsorbed moisture or gaseous molecules. The combustion of carbon begins around 300^{o}C.[37,41] Fe_3O_4 can be oxidized to Fe_2O_3 when heated in air,[37,41] and the theoretical weight increase is 3.45%, based on the chemical reaction $4\ Fe_3O_4 + O_2 \rightarrow 6\ Fe_2O_3$. From TGA analysis, the carbon content of carbon decorated Fe_3O_4 nanoparticle was estimated to be 0.43%.

Electrochemical performance of olive-like Carbon decorated Fe3O4 in lithium storage

The as-prepared olive-like carbon decorated Fe_3O_4 nanoparticle fabricated directly on a copper disc was used as an additive-free ready electrode and assembled into a coin-type cell directly and evaluated. The electrochemical properties of as prepared additive-free Fe_3O_4/C electrode are shown in Figure 5. Optical image of the additive-free carbon decorated Fe_3O_4 as a ready electrode for cell assembly is shown in the inset of Figure 5a. The charge-discharge profiles of the first two cycles at the current of 100 mA g^{-1} with a cutoff voltage window of 0.01−3.0 V are shown in Figure 5a. In the first discharge curve, two potential plateaus at about 0.9 and 0.8 V are observed, which can be ascribed to the formation of a Li–Fe–O compound, the conversion reaction of the Li–Fe–O compound to Fe^0 and formation of Li_2O matrix.[14, 15, 20, 38, 42] This profile is different from the first cycle discharge profile of Fe_2O_3 negative-electrode materials,[42] which has two potential plateaus at around 1.6 and 0.8 V versus Li^+/Li (Figure S6a in SI). For the precursor of Fe_2O_3/C, the potential plateau at around 1.6V can be ascribed to the intercalation of Li^+ into α–Fe_2O_3, and the other potential plateau at around 0.8 V is due to the formation of $Li_2(Fe_2O_3)$ and the reduction of Fe ions to Fe^0.[15,42,43] The difference between first cycle discharge profile of carbon decorated Fe_3O_4 (Figure 5a) and the precursor of Fe_2O_3/C materials (Figure S7a in SI) illustrates the different electrochemical reactions involved during the first cycle of Li insertion, which also indirectly proves the successful conversion from Fe_2O_3 to Fe_3O_4 by *in situ* partial carbothermic reduction. The voltage drop from below 0.8 to 0.01 V could be attributed to the formation of a solid electrolyte interphase (SEI) due to the decomposition of the solvent in the electrolyte.[11, 20, 23, 38, 42, 44]

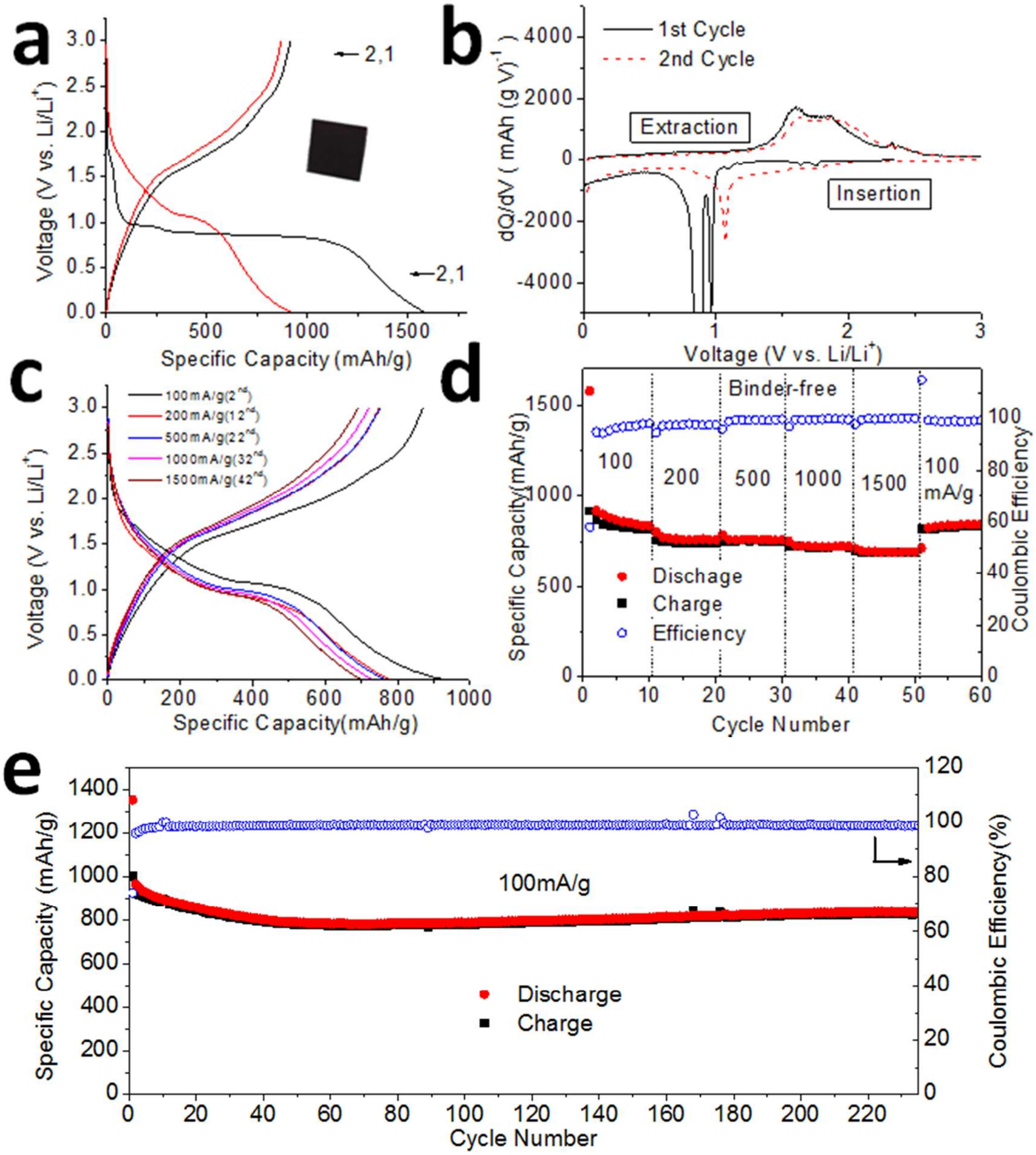

Figure 5. Electrochemical measurement of additive-free carbon decorated Fe_3O_4 fabricated directly on copper current collector: (a) first two cycle charge–discharge profiles; Inset of (a) shows the optical image of black additive-free Fe_3O_4 on a copper disc as a ready electrode; (b) differential capacity profiles for first two cycles; (c) Charge–discharge voltage profiles and (d) rate performances and Coulombic efficiency at different currents from 100 to 1500mAg^{-1}; (e) Cycling performance at 100 mA g^{-1}.

In the first cycle charge profile, the plateau around 1.7 V is attributed to the oxidation of Fe^0 to Fe^{2+} and Fe^{3+}.[44] The first cycle discharge and charge capacities are 1579 and 917 mA h g^{-1}, respectively. The irreversible capacity loss of around 42% could be attributed tothe decomposition of the electrolyte and formation of solid electrolyte interphase (SEI).[20] To better interpret the electrochemical reactions involved, the dQ/dV vs. V plots for the first two cycles are shown in Figure 5b, which matches well with plateaus discussed above. Additionally, the absence of the typical reduction peak at around 1.6 V widely observed for Fe_2O_3 proves that the electrode is based on Fe_3O_4.[17, 19, 42, 45, 46] In the 2nd cycle, both reduction and oxidation peaks are positively shifted as compared to the 1st cycle.

The charge–discharge voltage profiles at different currents of 100, 200, 500, 1000 and 1500mAg^{-1} are shown in Figure 5c, which are at the 2nd, 12th, 22nd, 32nd, and 42nd cycle, respectively. The charge–discharge voltage profiles at different currents almost overlap, which demonstrates the same reversible electrochemical reactions involved. The specific discharge capacities are 919, 772, 761, 752, and 727 mA h g^{-1} at currents of 100, 200, 500, 1000 and 1500 mA g^{-1}, respectively. As we can see, the capacity fades slowly at the currents from 200 to 1500 mA g^{-1}, which has rarely observed for metal oxides tested in LIBs. And even at a high current of 1500 mA g^{-1}, the specific discharge capacities can still be maintained at 727 mA h g^{-1}, which shows improved rate performance as-compared to most reported Fe_3O_4 nanomaterial based anodes.[15, 20, 22]

The rate performances of the additive-free Fe_3O_4/C electrode was evaluated by charge-discharge the battery cells at different current densities for 10 cycles interval (Figure 5d). The average Coulombic efficiency from the 2nd is as high as 98.92, which indicates the excellent electrochemical reversibility. The capacities are very stable and no distinguishable capacity drop can be observed at each current. It is interesting to highlight that no significant capacity drop observed when current was doubled, which suggests the electrodes could be used in fast charge LIBs. It is interesting to observe the specific capacity was recovered to 835.5mA h g^{-1} after 60 cycles, when the current was changed back to 100mA g^{-1}. More interestingly, we observe an increase of capacity after the current is recovered to 100mAg^{-1} from 1500mAg^{-1}. This could be explained by continuous activating process of the electrode.[7, 38, 47] Excellent cycling performance was achieved with a specific capacity at ~ 800 mA h g^{-1} for at least 175 cycles (Figure 5e). The superior electrochemical performances could be attributed to its porous structure induced good accessibility of Li^+ ions and improved strain accommodation and the way electrode prepared. In contrast, the conventional electrode prepared from the same Fe_3O_4/C demonstrated poor cycling performances (Figure S6 in SI), which indicates the critical role of electrode preparation. The olive-like shape could still be observed from the sample of Fe_3O_4/C nanoparticles after cycling, indicating relatively structural stability (Figure S8 in SI). As a comparison, the additive-free Fe_2O_3/C electrode shows very poor electrochemical performance (Figure S7 in SI).

4. Conclusions

In summary, porous olive-like carbon decorated Fe_3O_4 was successfully prepared from a precursor of porous olive-like Fe_2O_3/C nanoparticles. The precursor was obtained by a fast one-pot solvothermal method. A novel CAP method to prepare additive-free electrode was developed for the first time. The active materials were synthesized on current collector by CAD directly without any binder, conductivity enhancer or solvent employed. When tested as negative-electrode materials for LIBs, the additive-free olive-like Fe_3O_4/C electrode exhibited excellent electrochemical performances for lithium storage demonstrating its promising potential to be carbon alternatives for SIBs.

ASSOCIATED CONTENT

Supporting Information EDS of olive-like Fe_2O_3/C and Carbon decorated Fe3O4 nanoparticles; FESEM images of sample prepared with different amount of glucose; TGA of olive-like Carbon decorated Fe3O4; electrochemical performance of additive-free Fe_2O_3/C electrode; FESEM characterization after battery test. This information is available free of charge via the Internet at http://pubs.acs.org/.

References

1. J.-M. Tarascon and M. Armand, *Nature*, 2001, 414, 359-367.
2. M. Armand and J.-M. Tarascon, *Nature*, 2008, 451, 652-657.
3. L. Ji, Z. Lin, M. Alcoutlabi and X. Zhang, *Energy Environ. Sci.*, 2011, 4, 2682-2699.
4. A. S. Arico, P. Bruce, B. Scrosati, J. M. Tarascon and W. Van Schalkwijk, *Nat. Mater.*, 2005, 4, 366-377.
5. P. G. Bruce, B. Scrosati and J. M. Tarascon, *Angew. Chem., Int. Ed.*, 2008, 47, 2930-2946.
6. F. Cheng, J. Liang, Z. Tao and J. Chen, *Adv. Mater.*, 2011, 23, 1695-1715.
7. P. Poizot, S. Laruelle, S. Grugeon, L. Dupont and J. Tarascon, *Nature*, 2000, 407, 496-499.
8. F. Liu, S. Song, D. Xue and H. Zhang, *Nanoscale Res. Lett.*, 2012, 7, 149.
9. J. Zhu, K. Y. S. Ng and D. Deng, *ACS Appl. Mater. Interfaces*, 2014, DOI: 10.1021/am4055996.
10. N. Tsuda, *Electronic conduction in oxides*, Springer, 2000.
11. S. M. Yuan, J. X. Li, L. T. Yang, L. W. Su, L. Liu and Z. Zhou, *ACS Appl. Mater. Interfaces*, 2011, 3, 705-709.
12. Y. Chen, H. Xia, L. Lu and J. Xue, *J. Mater. Chem.*, 2012, 22, 5006-5012.
13. Q. Q. Xiong, J. P. Tu, Y. Lu, J. Chen, Y. X. Yu, Y. Q. Qiao, X. L. Wang and C. D. Gu, *J. Phys. Chem. C*, 2012, 116, 6495-6502.
14. P. L. Taberna, S. Mitra, P. Poizot, P. Simon and J. M. Tarascon, *Nat Mater*, 2006, 5, 567-573.
15. W. M. Zhang, X. L. Wu, J. S. Hu, Y. G. Guo and L. J. Wan, *Adv. Funct. Mater.*, 2008, 18, 3941-3946.
16. T. Muraliganth, A. Vadivel Murugan and A. Manthiram, *Chem. Commun.*, 2009, DOI: 10.1039/B916376J, 7360-7362.
17. J.-K. Hwang, H.-S. Lim, Y.-K. Sun and K.-D. Suh, *J. Power Sources*, 2013, 244, 538-543.
18. W. Wei, S. Yang, H. Zhou, I. Lieberwirth, X. Feng and K. Müllen, *Adv. Mater.*, 2013, DOI: 10.1002/adma.201300445, n/a-n/a.
19. S. Jin, H. Deng, D. Long, X. Liu, L. Zhan, X. Liang, W. Qiao and L. Ling, *J. Power Sources*, 2011, 196, 3887-3893.
20. T. Yoon, C. Chae, Y.-K. Sun, X. Zhao, H. H. Kung and J. K. Lee, *J. Mater. Chem.*, 2011, 21, 17325-17330.
21. Y. Piao, H. S. Kim, Y.-E. Sung and T. Hyeon, *Chem. Commun.*, 2010, 46, 118-120.
22. M. Zhang, D. Lei, X. Yin, L. Chen, Q. Li, Y. Wang and T. Wang, *J. Mater. Chem.*, 2010, 20, 5538-5543.
23. L. Wang, J. Liang, Y. Zhu, T. Mei, X. Zhang, Q. Yang and Y. Qian, *Nanoscale*, 2013, 5, 3627-3631.
24. C. He, S. Wu, N. Zhao, C. Shi, E. Liu and J. Li, *ACS Nano*, 2013, 7, 4459-4469.
25. L. Zhang, H. B. Wu and X. W. Lou, *Adv Energy Mater*, 2014, 4.
26. G. X. Gao, L. Yu, H. B. Wu and X. W. Lou, *Small*, 2014, 10, 1741-1745.
27. L. Zhang, H. B. Wu, R. Xu and X. W. Lou, *Crystengcomm*, 2013, 15, 9332-9335.
28. L. Zhang, H. B. Wu and X. W. Lou, *J Am Chem Soc*, 2013, 135, 10664-10672.
29. L. Zhang, H. B. Wu, S. Madhavi, H. H. Hng and X. W. Lou, *J Am Chem Soc*, 2012, 134, 17388-17391.
30. Z. Y. Wang, D. Y. Luan, S. Madhavi, C. M. Li and X. W. Lou, *Chem Commun*, 2011, 47, 8061-8063.
31. J. S. Chen, T. Zhu, X. H. Yang, H. G. Yang and X. W. Lou, *J Am Chem Soc*, 2010, 132, 13162-13164.
32. B. Wang, J. S. Chen, H. B. Wu, Z. Y. Wang and X. W. Lou, *J Am Chem Soc*, 2011, 133, 17146-17148.
33. B. Wang, H. B. Wu, L. Zhang and X. W. Lou, *Angew Chem Int Edit*, 2013, 52, 4165-4168.
34. Z. Wang, D. Luan, S. Madhavi, Y. Hu and X. W. Lou, *Energ Environ Sci*, 2012, 5, 5252-5256.
35. J. S. Chen, Y. M. Zhang and X. W. Lou, *Acs Appl Mater Inter*, 2011, 3, 3276-3279.
36. D. Deng and J. Y. Lee, *Chem Mater*, 2008, 20, 1841-1846.

37. T. Zhu, J. S. Chen and X. W. Lou, *J. Phys. Chem. C*, 2011, 115, 9814-9820.
38. L. Wang, J. Liang, Y. Zhu, T. Mei, X. Zhang, Q. Yang and Y. Qian, *Nanoscale*, 2013.
39. K. C. Chin, G. L. Chong, C. K. Poh, L. H. Van, C. H. Sow, J. Lin and A. T. S. Wee, *J. Phys. Chem. C*, 2007, 111, 9136-9141.
40. K. Charette, J. Zhu, S. O. Salley, K. Y. S. Ng and D. Deng, *RSC Advances*, 2014, 4, 2557-2562.
41. J. S. Chen, Y. Zhang and X. W. Lou, *ACS Appl. Mater. Interfaces*, 2011, 3, 3276-3279.
42. Z. Xiao, Y. Xia, Z. Ren, Z. Liu, G. Xu, C. Chao, X. Li, G. Shen and G. Han, *J. Mater. Chem.*, 2012, 22, 20566-20573.
43. J. Chen, L. Xu, W. Li and X. Gou, *Adv. Mater.*, 2005, 17, 582-586.
44. S. H. Lee, S.-H. Yu, J. E. Lee, A. Jin, D. J. Lee, N. Lee, H. Jo, K. Shin, T.-Y. Ahn, Y.-W. Kim, H. Choe, Y.-E. Sung and T. Hyeon, *Nano Letters*, 2013, 13, 4249-4256.
45. B. Wang, J. S. Chen, H. B. Wu, Z. Wang and X. W. Lou, *J. Am. Chem. Soc.*, 2011, 133, 17146-17148.
46. X. Zhu, Y. Zhu, S. Murali, M. D. Stoller and R. S. Ruoff, *ACS Nano*, 2011, 5, 3333-3338.
47. L. Qie, W.-M. Chen, Z.-H. Wang, Q.-G. Shao, X. Li, L.-X. Yuan, X.-L. Hu, W.-X. Zhang and Y.-H. Huang, *Adv. Mater.*, 2012, 24, 2047-2050.